



# Infiltration and permeability of porous ceramics simulated by random networks

Vladimir Mityushev<sup>1</sup> · Natalia Rylko<sup>1</sup> · Anna Janina Dolata<sup>2</sup> · Maciej Dyzia<sup>2</sup>

Received: 19 December 2023 / Revised: 24 April 2024 / Accepted: 29 April 2024 / Published online: 27 June 2024  
This is a U.S. Government work and not under copyright protection in the US; foreign copyright protection may apply 2024

## Abstract

A network computational model for a 3D ceramic structure is developed. The model is applied to study the impact of geometric and material parameters of structure on the liquid metal flow through random porous ceramic medium in pressure infiltration processes. The characteristic geometric features of the ceramic structure favorable for liquid metal flow during the infiltration process are determined. The method of structural approximation and constructive homogenization are applied, and the discrete stationary Stokes equations on random graphs are considered. This approach gives a robust algorithm to determine the macroscopic permeability  $K$  of interpenetrating phases. The dependencies of  $K$  on the distribution of connections (windows) between the cells (inclusions) are derived. The numerical simulations demonstrate that the permeability  $K$  does not depend on the scaled distribution sizes of windows. This implies that  $K$  is proportional to the mean value of the window areas. The considered model takes into account a random complex structure of 3D ceramic. Hence, it complements the previous study on the local transport properties of tubes (windows) connecting the cells.

**Keywords** Pressure infiltration · Random network · Permeability of porous medium · Liquid metal flow

## 1 Introduction

Metal matrix composites (MMCs) based on light metal alloys (i.e., Al, Mg) usually consist of a reinforcing phase in the form of particles [1] or short fibers [2]. This kind of widely known materials is obtained, in particular, by the stir casting method. A new solution in the area of MMCs is materials with percolating metallic and ceramic phases (i.e., IPCs—interpenetrating phase composites), widely described by Kota et al. [3]. Currently, IPCs are usually fabricated by

pressure infiltration methods (e.g., centrifugal infiltration [4], or gas pressures' infiltration [5]). The ceramic phase in the form of porous skeletons has significant potential for the next-generation engineering applications [3]. The reinforcing elements of IPCs form a spatially ordered and random ceramic skeleton with complex topological and geometric features. Porous ceramics, also called cellular ceramics, are a relatively new and prospective material due to their special properties [6], such as low relative weight, high hardness, high temperature resistance, and specific damage mechanism (microcracks' propagation). These properties affect the energy absorption and dispersion capacity, which can be increased using foam materials with an open-cell structure. Porous ceramic skeletons, nowadays, have many applications as final products (i.e., filters used for thermal gas separation) or lightweight structural components. As opposed to the conventional dense counterparts, this kind of material can be infiltrated through an elastomer [7] or metal alloy [4, 8] to form functional composites in which each phase forms a fully interconnected network. Their design focuses on obtaining much higher physico-mechanical properties compared to unreinforced materials (i.e., metals, polymers), as well as classic composites reinforced with particles or fibers.

✉ Anna Janina Dolata  
anna.dolata@polsl.pl

Vladimir Mityushev  
vladimir.mityuszew@pk.edu.pl

Natalia Rylko  
natalia.rylko@pk.edu.pl

Maciej Dyzia  
maciej.dyzia@polsl.pl

<sup>1</sup> Faculty of Computer Science and Telecommunications,  
Cracow University of Technology, Warszawska St. 24,  
31-155 Kraków, Poland

<sup>2</sup> Faculty of Materials Engineering, Silesian University  
of Technology, Krasińskiego 8, 40-019 Katowice, Poland

The porous ceramic structure, the reinforcement phase, is important in their construction.

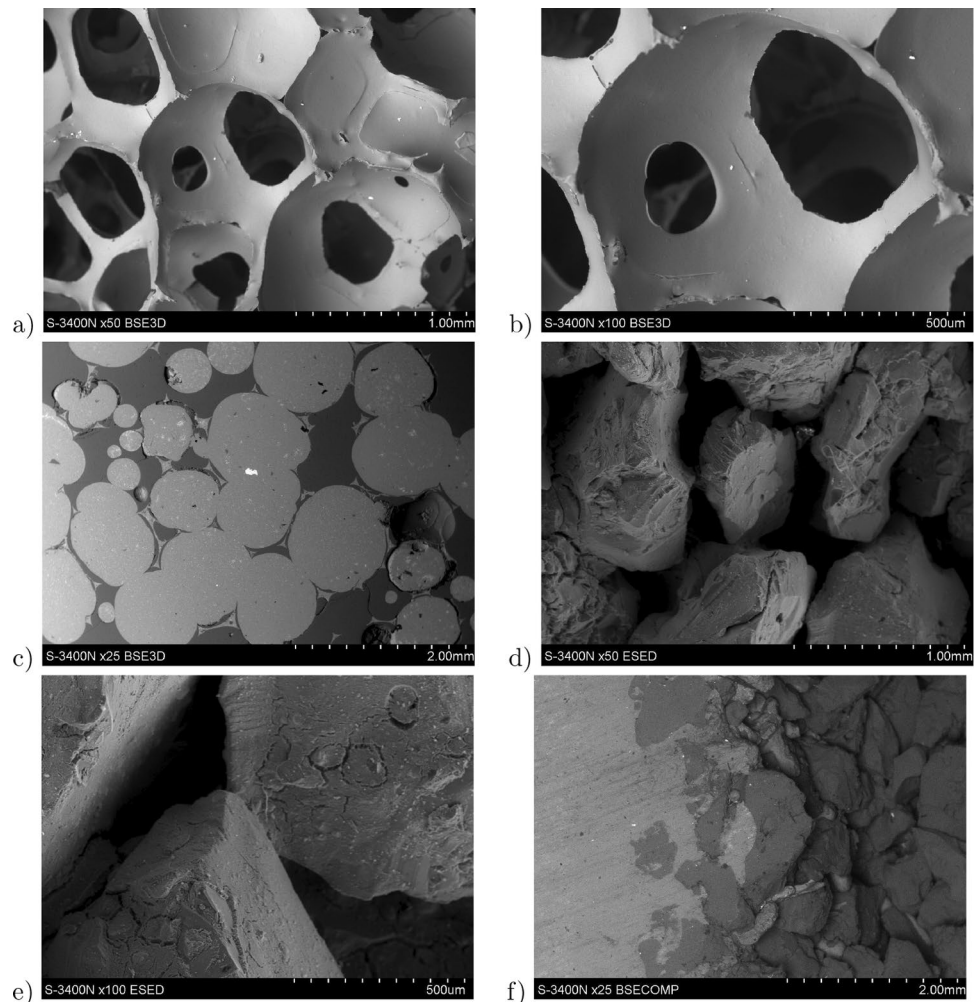
Both Colombo et al. [9] and Studart et al. [10] showed that advances in manufacturing methods now offer the possibility to fabricate cellular ceramics with a wide range of morphology and properties. To obtain the expected characteristics, the development of a specific structure with controlled volume fraction, size, type, and geometry of pores is required [11]. It should be noted that the density, porosity, absorbability, and permeability of porous ceramic skeletons are the key macroscopic parameters influencing the efficiency of the infiltration process. These averaged characteristics and physical properties of alumina skeletons were estimated in the previous experimental works [4, 12, 13]. Based on the obtained results, both theoretical and experimental, it was noted that besides the above parameters, the geometric properties of the structure strongly impact the success or failure of the infiltration process (Fig. 1). This structural problem requires a new subtle and advanced model taking into account the random distributions of components (cells or chamber) connected by microtubules to find the proper

key parameters and to determine their impact on infiltration quantitatively.

Following this task, we consider a class of IPCs generated by a regular structure resembling the hexagonal close-packed (hcp) lattice [14]. At the same time, the cells are chaotically connected by windows. A connected set of cells can be considered as a curvilinear channel, but only locally. The channels branch out and form a complex network. Various mathematical models and methods related to injection were developed for fluid through a curvilinear channel. A perturbation method was applied in [15] to curvilinear 3D channels. Multilayer modeling of lubricated contacts was developed in [16]. Optimization of flow in complex channels was discussed in [17]. These models are based on the analytical-numerical solution to PDE and the estimation of the local flow in an element of the porous medium.

We are interested in IPCs, which can be considered random porous media of cells connected by channels when a representative volume element with the corresponding complex geometry is simulated, and its macroscopic properties are estimated. Therefore, infiltration can be studied in the

**Fig. 1** Skeleton structure in various scales. Overlapping cells bounded by ceramic spheres are connected by windows (throats), as shown by dark spots. A viscous fluid occupies the cells and windows. Morphology of  $\text{Al}_2\text{O}_3$  ceramic preforms (skeletons) and effect of infiltration with liquid Al alloy, SEM: **a** and **b**  $\text{Al}_2\text{O}_3$  (*R*)—obtained by replacement of porous polymer matrix with total porosity at a level of 84%; **c** microstructure of Al/ $\text{Al}_2\text{O}_3$  composite; **d** and **e**  $\text{Al}_2\text{O}_3$  (*S*) prepared by sintering of ceramic powder with total porosity at a level of 50%; **f** microstructure of Al/ $\text{Al}_2\text{O}_3$  (*S*) composite with blocked infiltration. The units are shown on the right side at the bottom strip of each picture. The unit segment equals to: **a** 1 mm, **b** 500  $\mu\text{m}$  = 0.5 mm, **c** 1 mm, **d** 1 mm, **e** 500  $\mu\text{m}$  = 0.5 mm, **f** 2 mm



framework of the theory of homogenization [18] and its constructive applications to fluids [19], in particular, to filtration through porous media [20]. Extensions to high-frequency flow can be found in [21] and long-wave asymptotics in [22]. Non-Newtonian fluids in porous media were discussed by Farina et al. [23], and the advanced numeric computations were presented by Adler et al. [24]. The permeability of fractures, fracture networks, and fractured porous media was systematically investigated by Mourzenko et al. [25], including the continuous percolation described in [26]. Moreover, the classic percolation theory was systematically applied by Hunt et al. [27] to describe the percolation theory for flow in porous media.

In the present paper, we develop two mathematical approaches based on graph theory, which were applied separately to porous media and composites in the previous works. One of the first random network model of porous media was proposed in [28] where a series of several unit cells connected in parallel was considered. The flow problem through each unit cell was reduced to determining the flow in a tube. The porous medium was modeled by a network of cells connected through windows, and it is approximated to be a network of tubes. The network skeleton was simulated by randomly removing several windows in [29]. Further investigations led to the DeProF hybrid mechanistic-stochastic model for two-phase flow in porous media summarized in [30] and discussed in [31] for metal filtration, in [32] for carbonate rock, and in [33] for two-phase flow. The discussed random network model is used in the oil and gas industry to determine the permeability of porous media. This model is similar to the infiltration problem of IPCs. The outlined works primarily emphasize using a single pore flow as a building block for studying macroscopic flow.

As demonstrated in [34], accurate estimation of macroscopic permeability in a random structure requires careful investigation. In this regard, the computational theory of random homogenization outlined in [35] proves valuable. The corresponding graph model relies on the variational method of structural approximation [36], and asymptotic investigations [37]. The random graph simulations were performed in [38]. The structural approximation stands out among numeric approximations because of the following features. A discrete network and its elements (vertices and edges) correspond to the geometry of the porous medium and the expected domains of higher intensity flow.

In the present paper, we develop the structural approximation to investigate the impact of geometrical parameters (porosity, pore size, window size, etc.) on the transport properties of porous ceramics. The considered random Voronoi tessellations are tailored to meet the processes in IPCs and differ from the classic study [39]. The main simulated parameter is the macroscopic permeability  $\mathbf{K}$ . The impact of the IPC structures is systematically investigated on the

principal component of  $\mathbf{K}$ . The study follows the discrete homogenization procedure and determines the macroscopic properties of IPCs. This is of great importance in the case of gas infiltration technology, where the use of low gas pressure acting on the liquid metal does not damage the brittle ceramic structure.

## 2 Geometry

We now outline the representative volume element (RVE) conception of the considered media. According to the theory of homogenization, the effective permeability of the medium can be appropriately determined through a periodic cell problem with a given pressure jump per cell  $Q$  [18, 40]. The term “cell” means the rectangular cuboid  $Q$  in the homogenization theory. In the present paper, we use the term cell for a sphere and the term sample for the cuboid  $Q$  containing a set of spheres following the terminology of IPCs.

We shall follow the lines of linear [40] and nonlinear random composites [41] and develop the corresponding theory of infiltration of statistically homogeneous samples. RVE has to satisfy the conditions expressed by the representativeness in a statistical context. A random composite is a statistically homogeneous medium invariant under translations in space. A lattice group generated by three fundamental translation vectors is assigned to any fixed random statistically homogeneous composite. Therefore, an RVE exists that represents random non-periodic statistically homogeneous composites. A constructive method to determine RVE for dispersed composites is outlined in [42] for conductive composites and in [35] for suspensions. It is based on the structural sums and advanced simulations of samples to fulfill the condition of statistical homogeneity rigorously.

Consider 27 equal spheres, a fragment of the famous hcp lattice [14], displayed in Fig. 2a. All the geometrical and physical scales are dimensionless. The spheres are located in the cuboid  $\{(x, y, z) : -1 < x, y < 1, -2 < z < 2\}$ . We have three layers by 7 spheres on the planes  $z = 0, \pm 2\sqrt{\frac{2}{3}}$  and two layers by 3 spheres on the planes  $z = \pm\sqrt{\frac{2}{3}}$ . The centers of 7 spheres on the level  $z = 0$  are  $(0, 0, 0), (\pm 1, 0, 0), (\pm\frac{1}{2}, \pm\frac{\sqrt{3}}{2}, 0)$ . The coordinates of other centers are obtained by replacing the third coordinate by  $z = \pm 2\sqrt{\frac{2}{3}}$ . The centers of triples spheres on the level  $z = \pm\sqrt{\frac{2}{3}}$  are  $(0, -\frac{1}{\sqrt{3}}, \pm\sqrt{\frac{2}{3}}), (\pm\frac{1}{2}, \frac{1}{2\sqrt{3}}, \pm\sqrt{\frac{2}{3}})$ . It is convenient to numerate the centers  $\mathbf{x}_i = (x_i, y_i, z_i)$ ,  $i = 1, 2, \dots, 27$ , for instance, as in Fig. 2b.

The radius of spheres is equal to  $\frac{1}{\sqrt{3}}$ . Then, every triple of overlapping spheres does not have an empty space between

**Fig. 2** **a** RVE containing 27 overlapping spherical elements. **b** An incomplete Delaunay graph corresponding to the structure **a** with the enumerated vertices

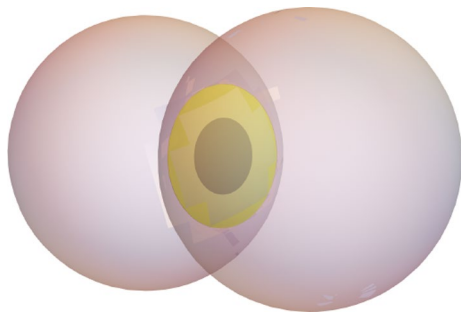
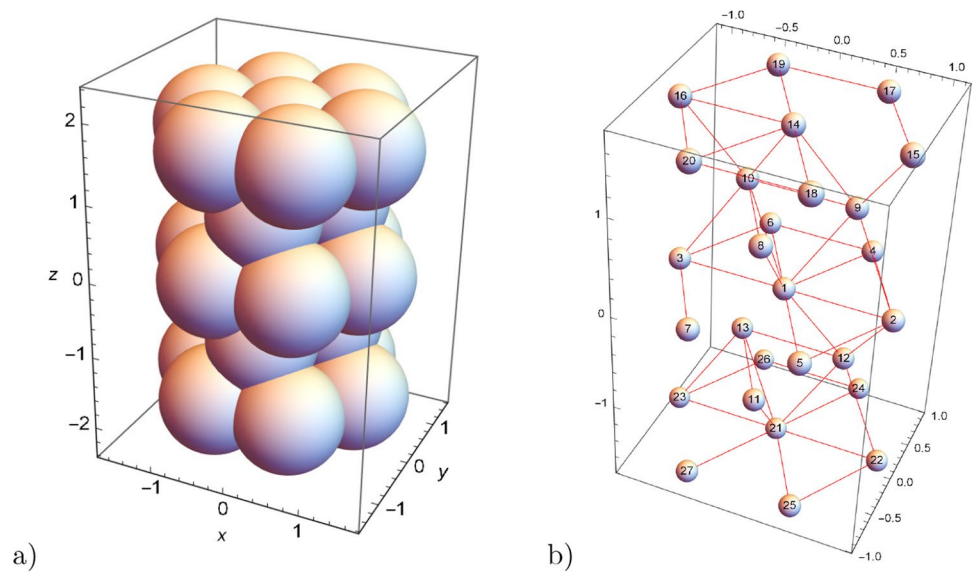


**Fig. 3** Two neighbor spheres overlapping over the circle. The disk  $D$  (yellow) is the joint boundary of two cells, each of them a part of the corresponding ball. The window  $W$  between the cell, a part of  $D$ , is shown by dark yellow

them. Every pair of neighbor spheres overlaps over a circle of radius  $\frac{1}{2\sqrt{3}}$ . Each circle bounds a disk. This disk  $D$  contains a smaller disk  $W$  called window and is considered the joint boundary of two new cells obtained from the considered spheres by deleting the corresponding spherical caps; see Fig. 3. In particular,  $D$  may coincide with  $W$ .

It is assumed that the structures considered in Fig. 1 are represented by a set of non-overlapping cells displayed in Fig. 2. Every cell is a part of the corresponding ball. It is bounded partially by the sphere and by the disks  $D$ . This construction repeats the Voronoi diagram [43] for the set of centers of spheres. The cells form the Voronoi partition of space. Only 27 finite cells of this partition are considered. A window may be located on the joint disk of two neighboring cells.

We now model the considered structure by a graph. The graph  $(V, E)$  consists of the vertices  $V$  connected by the edges

$E$ . It is assumed that the set  $V$  coincides with the set of centers of all 27 spheres. Two vertices are connected by an edge if a window is assigned between two corresponding cells. Therefore, the graph  $(V, E)$  corresponds to a structure of connected or disconnected cells. Following analogous two-dimensional investigations [38], we call  $(V, E)$  by the incomplete Delaunay graph. The graph  $(V, E)$  is called the complete Delaunay graph if a window is assigned to every pair of neighbor cells. An example of the graph  $(V, E)$  is displayed in Figs. 2b and 4.

Let  $\Omega$  denote the union of all the cells. The two-dimensional boundary  $\partial\Omega$  (skeleton) of the spatial domain  $\Omega$  consists of the outer boundary of all the spheres and the disks  $D$ , which do not contain windows, i.e.,  $D$  is a partition. Moreover, if a disk  $D$  contains a window  $W$  of disk form, the ring  $D \setminus W$  belongs to  $\partial\Omega$ . It is worth noting that the domain  $\Omega$  is not necessarily connected.

### 3 Method of structural approximation

The continuum model of infiltration can be based on the Stokes equations. Though infiltration is a dynamic process with the front of infiltration, the macroscopic permeability of RVE can be considered the critical infiltration parameter.

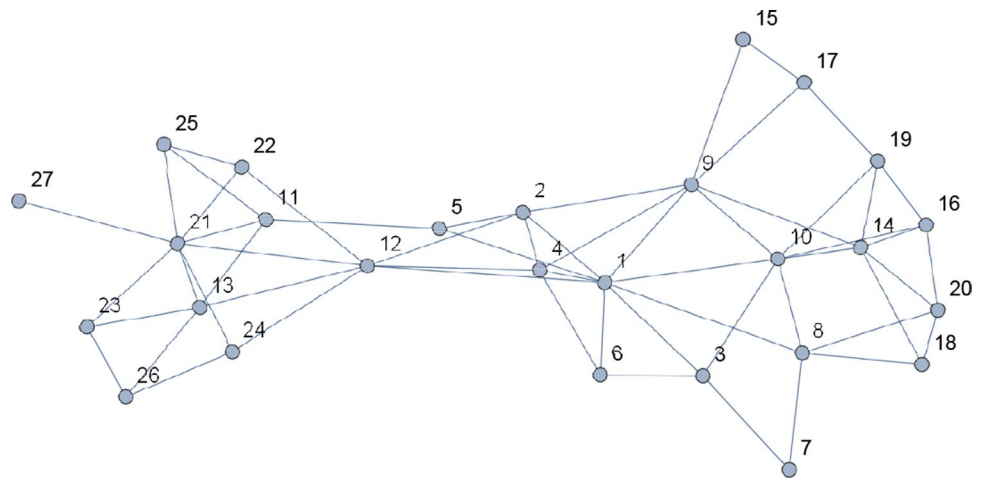
Consider a viscous fluid of the constant viscosity  $\mu$  in the domain  $\Omega$ . Let  $\mathbf{x} = (x, y, z)$  denote the spatial coordinate,  $\mathbf{v}(\mathbf{x})$  the velocity, and  $p(\mathbf{x})$  the pressure. Using the standard designation for the gradient operator  $\nabla$ , one can write the stationary Stokes equations in the form

$$\mu \nabla \mathbf{v} = \nabla p, \quad \nabla \cdot \mathbf{v} = 0 \quad \text{in } \Omega. \tag{1}$$

Let  $S^+$  and  $S^-$  denote the top and bottom parts of the surface  $\partial\Omega$ . For instance,  $S^+$  can be defined as the part of  $\partial\Omega$  visible from the top of the RVE displayed in Fig. 2. Therefore,  $\partial\Omega$



**Fig. 4** The standard plane graph isomorphic to the graph displayed in Fig. 2b. The considered graph is connected. An incomplete Delaunay graph may be disconnected



is decomposed on  $S^+$ ,  $S^-$  and the lateral part and the interior partitions  $S$ , i.e.,  $\partial\Omega = S^+ \cup S^- \cup S$ .

Let the averaged pressure gradient be given along the  $z$ -axis. The boundary conditions for the symmetric sample  $Q$  can replace the periodicity conditions. The normalized pressure  $p(x)$  can be fixed in the top and bottom faces of  $Q$  equal to 1 and 0, respectively. The velocity  $v(x, y, z)$  is a triply periodic function vanishing on the boundary  $\partial\Omega$ . The corresponding boundary and periodicity conditions keep their form after the transition to the discrete problem for a graph. Therefore, we have the following boundary condition on the normalized pressure

$$p(\mathbf{x}) = 1, \quad \mathbf{x} \in S^+; \quad p(\mathbf{x}) = 0, \quad \mathbf{x} \in S^-. \tag{2}$$

The velocity satisfies the non-slipping boundary condition

$$\mathbf{v}(\mathbf{x}) = \mathbf{0}, \quad \mathbf{x} \in S. \tag{3}$$

In the considered case, the periodic problem is reduced to the boundary value problem (1)–(3). This is the classic boundary value problem for the Stokes equation [44]. Let us know its solution. Then, the permeability of the medium  $K$  occupying the domain  $\Omega$  in the  $z$ -direction is defined by the volume integral [24]

$$K_z = \frac{\mu l}{\Delta p} \int_{\Omega} v_z \, d\mathbf{x}, \tag{4}$$

where  $v_z$  is the  $z$ -component of  $\mathbf{v}$ ,  $\Delta p$  is the difference of pressures equal to 1, and  $l$  is the thickness of the bed equal to 4 in our case.

Consider a class of media represented by domains  $\Omega$ . Let  $\Omega^{\max}$  be the maximally possible domain with all the windows having the maximally possible area of windows. This medium has the maximal permeability denoted by  $K_z^{\max}$ . We will use the dimensionless permeability  $K$  respective to

$K_z^{\max}$ ; more precisely, the normalized permeability is introduced as

$$K = \frac{\int_{\Omega} v_z \, d\mathbf{x}}{\int_{\Omega^{\max}} v_z^{\max} \, d\mathbf{x}}. \tag{5}$$

We now proceed to pass to a discrete model of permeability based on the structural approximation. The method of structural approximation is similar to a finite-element method but closely related to the structure of the medium. For instance, in the considered case, the element is a cell, and the mesh is represented by the Delaunay graph introduced in the previous section. The method has been applied to various mechanical problems. A rigorous justification of the method was established in [37] by asymptotic methods and in [36] by a variational method.

Following the method of structural approximation, we introduce the pressure  $p_i$  averaged over the  $i$ th cell ( $i = 1, 2, \dots, 27$ ). The Delaunay graph  $(V, E)$  determines the structure and represents the domain  $\Omega$  with windows. The boundary conditions (2) become

$$p_i = 1 \text{ for } i = 14, 15, \dots, 20; \quad p_i = 0, \text{ for } i = 21, 22, \dots, 27, \tag{6}$$

where the vertices' numeration shown in Figs. 2b and 4 is used. The pressure  $p$  is represented by the values  $p_i$  satisfying the discrete Laplace equation [45]

$$p_i = \frac{1}{d_i} \sum_{j \sim i} p_j, \quad i = 1, 2, \dots, 13. \tag{7}$$

Here, the relation  $j \sim i$  means that the vertices  $i$  and  $j$  are connected;  $d_i$  stands for the degree of the  $i$ th vertex, i.e., the number of edges connecting the  $i$ th vertex with others. If  $d_i = 0$ , the vertex  $i$  is isolated and excluded from the system of equations (7).

The linear algebraic system (7) has a unique solution [45]. Let the values  $p_i$  be calculated. The velocity vector  $\mathbf{v}_l$  is determined on every edge connecting the vertices  $i$  and  $j$  with the coordinates  $\mathbf{x}_i$  and  $\mathbf{x}_j$ , respectively, by the formula

$$\mathbf{v}_l = -\frac{K_{\text{edge}}}{\mu}(p_j - p_i)\frac{\mathbf{x}_j - \mathbf{x}_i}{|\mathbf{x}_j - \mathbf{x}_i|}, \quad i, j = 1, 2, \dots, 27. \quad (8)$$

Here,  $K_{\text{edge}}$  denotes the permeability of an edge. In the theory of graphs,  $K_{\text{edge}}$  is usually proportional to the inverse value of  $|\mathbf{x}_j - \mathbf{x}_i|$ . In the considered case, all the edges have the same length. Hence,  $K_{\text{edge}}$  is a constant for all edges, not impacting the dimensionless macroscopic permeability. The ultimate respective permeability is calculated employing the  $z$ -components of  $\mathbf{v}_l$

$$K = -\frac{1}{K_0} \sum_{(i,j) \in E} v_{lz}. \quad (9)$$

The sum is taken over all the edges of graph  $(V, E)$ . The normalization constant  $K_0$  is calculated in the next section.

## 4 Implementation of algorithm

### 4.1 General

The method of structural approximation yields the algorithm summarized in the previous section for a fixed graph  $(V, E)$ . The algorithm was implemented with the package Mathematica®, which contains the built-in operator `Solve` applied to eq. (7) and others on the graph characteristics such as adjacency matrix and vertex degree. In the developed model of random media, the set of vertices  $V$  is fixed; the coordinates of  $V$  are written at the beginning of Sect. 2. The edges  $E$  are randomly generated. The main key of implementation is the procedure of random simulation of edges representing windows.

### 4.2 Equal windows

Consider the complete Delaunay graph  $(V, E^{\text{max}})$ . Application of the algorithm yields the pressure distribution shown in Fig. 5. This result easily follows from the symmetry of the graph  $(V, E^{\text{max}})$  and the symmetric boundary conditions for pressure. The pressure changes with the five layers from the top to the bottom of RVE as  $p = 1, 0.75, 0.5, 0.25, 0$ .

The  $z$ -component of the velocity on edges is calculated by (8). It is the same on every edge and equal to  $v_{lz} = -\frac{K_{\text{edge}}}{\mu}0.25$ . The number of edges connecting four different layers is equal to 36. Then, the formula (9) yields the dimensionless macroscopic permeability  $K_z^{\text{max}} = \frac{9K_{\text{edge}}}{K_0\mu}$ . This equation determines the normalization constant  $K_0 = \frac{9K_{\text{edge}}}{\mu}$ . Therefore, the dimensionless permeability  $K = K(V, E)$  for a graph  $(V, E)$  is normalized in such a way that the maximal possible permeability for the complete Delaunay graph holds  $K(V, E^{\text{max}}) = 1$  and the permeability  $K = K(V, E)$  is defined, respectively, to this maximal value. The normalized  $z$ -component of the velocity is calculated by the following formula from (8):

$$v_{lz} = -(p_j - p_i)\frac{z_j - z_i}{|\mathbf{x}_j - \mathbf{x}_i|}, \quad i, j = 1, 2, \dots, 27, \quad (10)$$

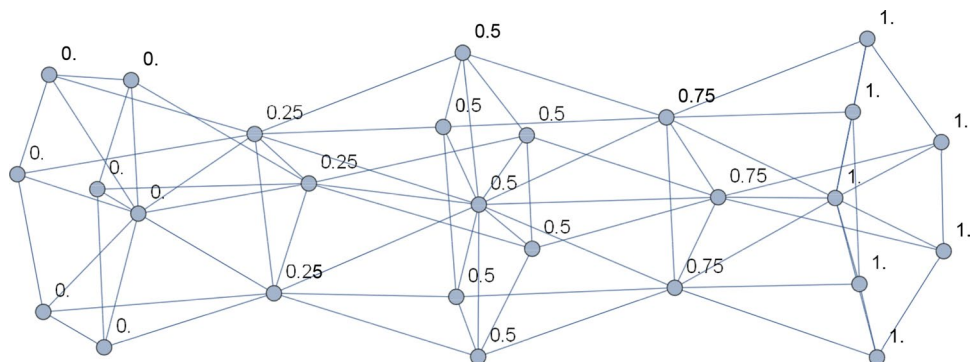
where  $\mathbf{x}_i = (x_i, y_i, z_i)$  denotes the spatial coordinate of the  $i$ th center. The normalized permeability is found by the normalized equation (9)

$$K = - \sum_{(i,j) \in E} v_{lz}. \quad (11)$$

The established normalization clarifies the algorithm to determine  $K = K(V, E)$  in the deterministic statement for each fixed graph  $(V, E)$ .

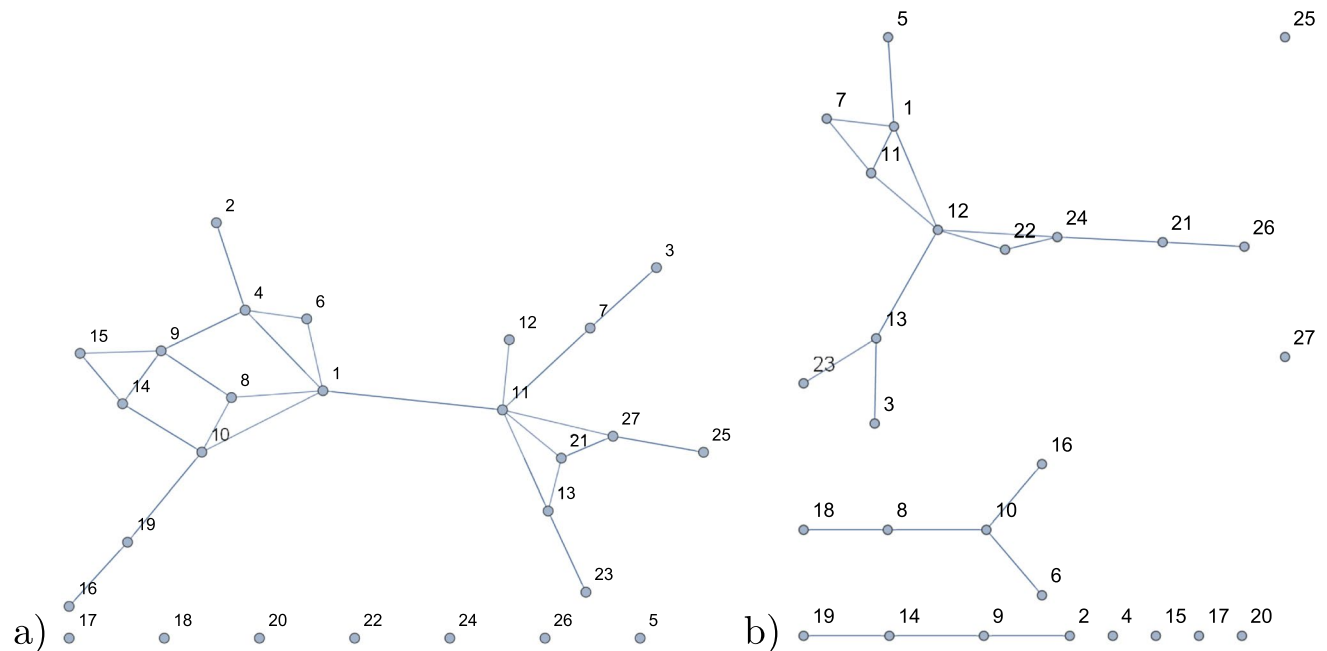
We are now ready to precisely introduce the random simulation of graphs with the fixed vertices  $V$  and the randomly selected edges  $E$ . Introduce the adjacency matrix  $A^{\text{max}}$  of the complete Delaunay graph  $(V, E^{\text{max}})$ . The element of this matrix  $a_{ij}^{\text{max}}$  ( $i, j = 1, 2, \dots, 27$ ) is equal to 1 if the vertices  $i$

Fig. 5 The standard plane graph  $(V, E^{\text{max}})$  of the pressure values at vertices



and  $j$  are connected and equal to 0 otherwise. Consider now a random set  $E$  defined by the probability of connection  $P$ , i.e.,  $P$  expresses the probability of a window between two neighbor cells. Let an edge be deleted with the probability  $(1 - P)$  from  $E^{\max}$ . As a result, we get a set of edges  $E$ , hence a new graph  $(V, E)$ . This random process is implemented by 100 computer experiments. Actually, we have the set of graphs  $(V, E_s(P))$  ( $s = 1, 2, \dots, 100$ ) simulated 100 times with the fixed  $P$ . The probability  $P = 0.025n$  ( $n = 1, 2, \dots, 40$ ) is taken in simulations. It is convenient to work with the adjacency matrix  $A$  of the Delaunay graph  $(V, E)$  where the element of this matrix has the form  $a_{ij} = a_{ij}^{\max} X_{ij}$ . Here, the random variables  $X_{ij}$  take the value 1 with the probability  $P$  and 0 with the probability  $(1 - P)$ . The value  $X_{ij}$  is simulated independently for every pair  $(i, j)$  with  $i > j$  and  $X_{ji} = X_{ij}$ . The diagonal elements vanish,  $a_{ii} = 0$ . In the extreme cases, we get the complete Delaunay graph  $(V, E_s(1)) = (V, E^{\max})$  and the degenerate graph with isolated vertices  $(V, E_s(0)) = (V, \emptyset)$  for any realization  $s$ . Here,  $\emptyset$  stands for the empty set.

Figures 2b and 4 display a randomly generated connected graph for  $P = 0.7$ . Figure 6 displays two disconnected graphs for  $P = 0.3$ . The left graph (a) contains a path connecting the top vertex 14 with the bottom vertex 21. Hence, this graph has a positive permeability, though it includes isolated vertices 17, 18, ... (dead flow regions). The permeability of the right graph (b) vanishes, since the top and bottom points are not connected.



**Fig. 6** Two plane graphs **a** and **b** generated by the same code with  $P = 0.3$ . The vertex 15 from the top and the vertex 21 from the bottom displayed in Fig. 2b are connected in the left graph by the path (14, 9, 8, 1, 11, 21). The top and bottom layers are not connected in the right graph

The permeability of graphs  $(V, E_s(P))$  can be expressed in the graph's percolation chains and isolated components. We say that a graph  $(V, E_s(P))$  is permeable if a chain exists connecting a top point ( $p = 1$ ) with a bottom point ( $p = 0$ ). Figure 7 displays the dependence of the statistical

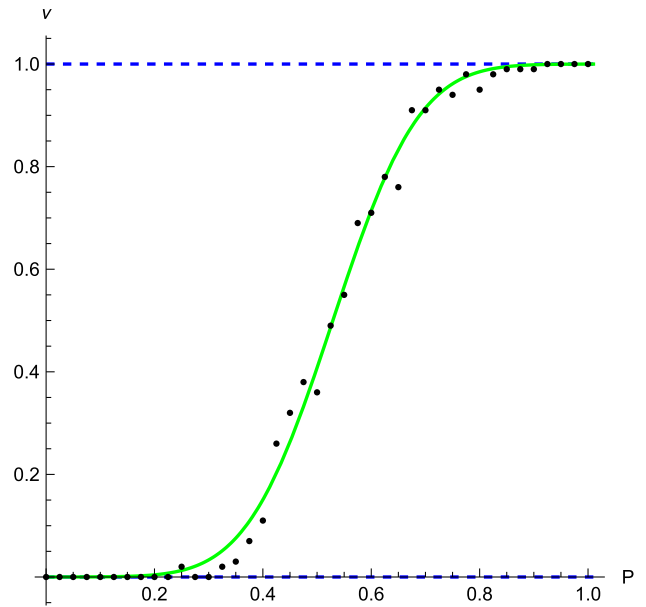
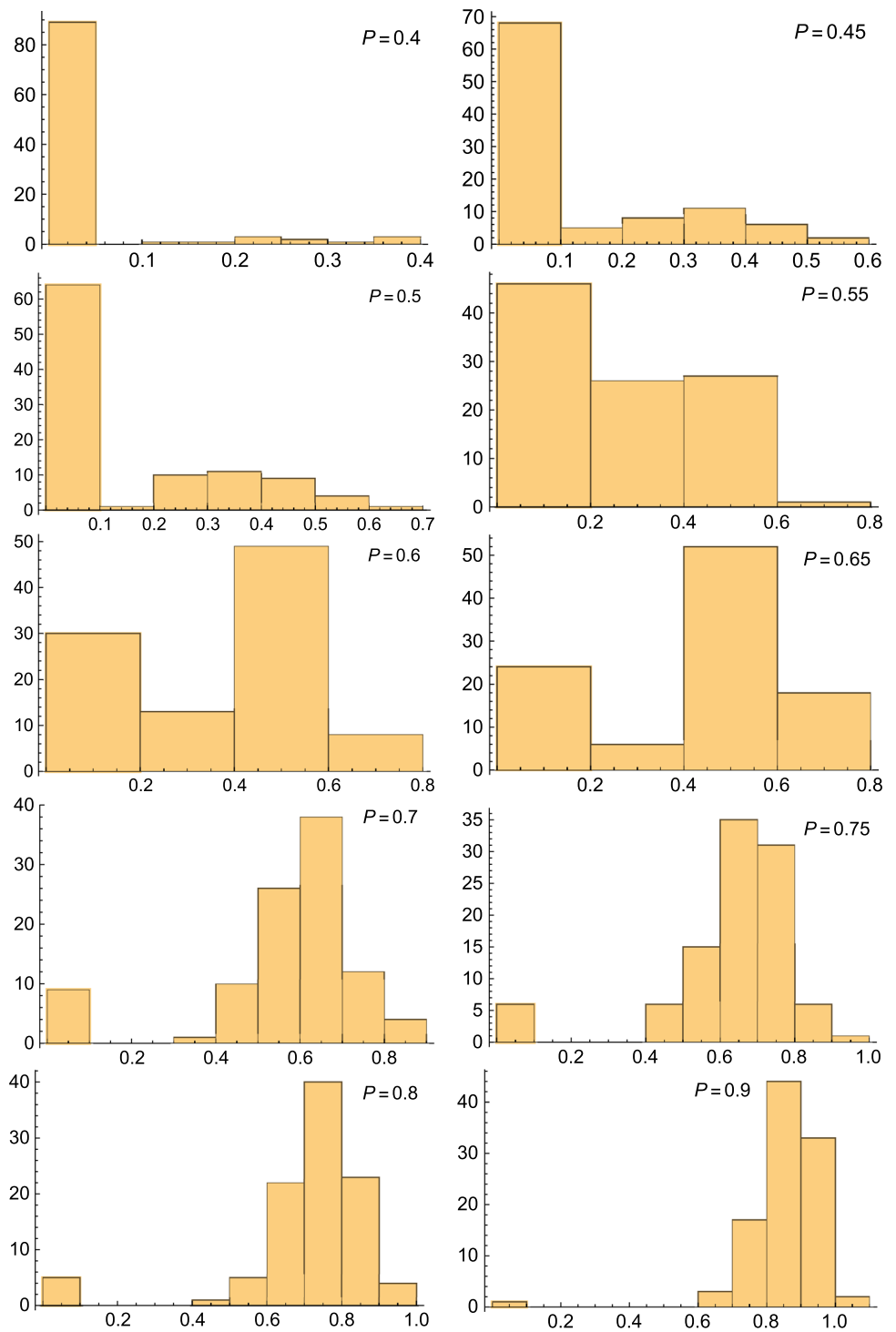


**Fig. 7** The statistical frequency of permeable graphs  $\nu$  on the probability  $P$ . Data are shown by points; the function (12) by solid (green) line

**Fig. 8** Distribution of permeability of 100 graphs for a fixed  $P$ . The normalized permeability  $K$  lies on the horizontal axis and its frequency  $\nu_K$  on the vertical axis



frequency of permeable graphs  $\nu$  on the probability  $P$ . The value  $\nu$  shows the share of permeable graphs in 100 randomly simulated graphs with a fixed  $P$ . The solid (green) graphics of the error-type function

$$\nu(P) = \frac{1}{2} - \frac{1}{\sqrt{\pi}} \int_0^{3-5.66P} \exp(-t^2) dt \tag{12}$$

fits the discrete data.

The implemented algorithm yields the statistical estimations of the permeability of graphs  $(V, E_s(P))$  and its



**Table 1** The statistical data of permeability  $K = K(V, E_s(P))$  averaged over 100 numerical experiments, the empirical mean value  $\mathbb{E}[K]$ , and the standard deviation  $\mathbb{D}[K]$  of  $K$  for a fixed  $P$

$P$	$\mathbb{E}[K]$	$\mathbb{D}[K]$
0.40	0.029572	0.088991
0.45	0.104312	0.164493
0.50	0.135862	0.194654
0.55	0.223127	0.214618
0.60	0.349568	0.242041
0.65	0.420890	0.253500
0.70	0.560500	0.198916
0.75	0.630944	0.188600
0.80	0.707188	0.185678
0.85	0.797430	0.116747
0.90	0.854727	0.112784

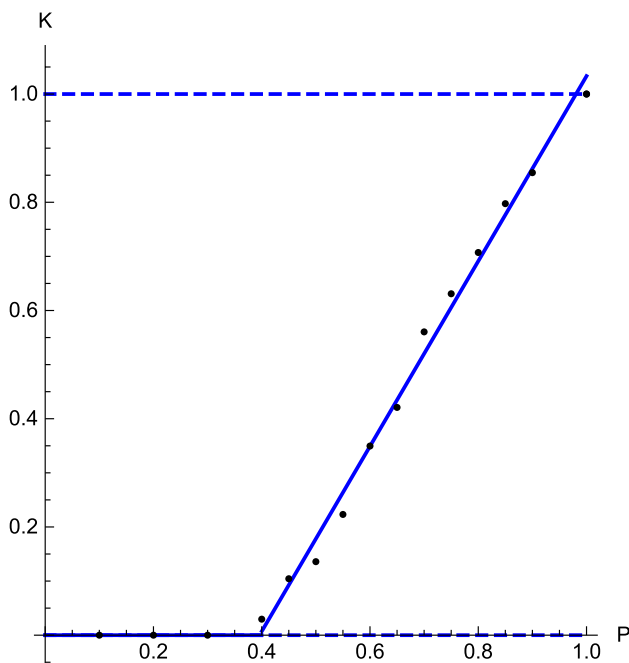


**Fig. 9** The dependence of the averaged permeability from Table 1 on the window probability  $P$ . The linear function (13) fits the points on the interval (0.4, 1)

dependencies on  $P$ . The results of simulations are presented in Figs. 8 and 9. We are interested in the frequency values of  $K$  denoted below as  $v_K$ . The frequency distributions of  $K$  for  $P = 0.4, 0.45, 0.5, \dots, 0.9$  are selected in the histograms of Fig. 8. The permeability  $K$  strongly vanishes except for a few statistical realizations for  $P \leq 0.4$ , i.e., the frequency  $v_K$  is maximal for  $K$  near zero. At the same time, the maximal frequency  $v_K$  distances from 1 for large  $P \geq 0.75$ . It is worth noting that all the considered frequency distributions include the local peak at the zero frequency. The second peak is located a little bit left to  $P$ . For instance, the histogram

$P = 0.65$  has the peak  $v_K = 53$  at the interval  $0.4 \leq K < 0.6$ . The second peak  $v_K = 24$  is achieved at  $0 \leq K < 0.2$ . The vanishing frequency  $v_K$  is not shown for  $K > K_c(P)$ , where  $K_c(P)$  denotes the maximal permeability with the positive frequency. For instance,  $K_c(0.4) = 0.4, K_c(0.45) = 0.6$  etc.

The frequencies  $v$  in Fig. 7 and  $v_K$  in Fig. 8 have different meanings. The value  $v$  characterizes the share of connected graphs,  $v_K$  the permeability. Both frequencies are considered as functions on the probability  $P$ .

The following linear function fits the points on the interval (0.4, 1) from Table 1:

$$K = -0.677027 + 1.71024P. \tag{13}$$

One can observe an excellent agreement of the line (13) with the point data.

### 4.3 Random size windows

In the present section, we modify the algorithm and the corresponding implementation to the case of different areas of windows. The modification consists in the introduction of the mutually independent random variables  $S_{ij}$  uniformly distributed on the interval  $(q_{\min}, 1)$ . The variable  $S_{ij}$  establishes the respective size of the window along the edges connecting the vertices  $i$  and  $j$ . The formula for the permeability (11) is modified by the introduction of multipliers

$$K = - \sum_{(i,j) \in E} S_{ij} v_{Lz}. \tag{14}$$

It is worth noting that the discrete random variable  $X_{ij}$  takes two values: 0 and 1. The value  $X_{ij} = 0$  blocks the flow between the cells  $i$  and  $j$ . The continuous random variable  $S_{ij}$  does not vanish for  $q_{\min} > 0$ . It scales the velocity between the cells.

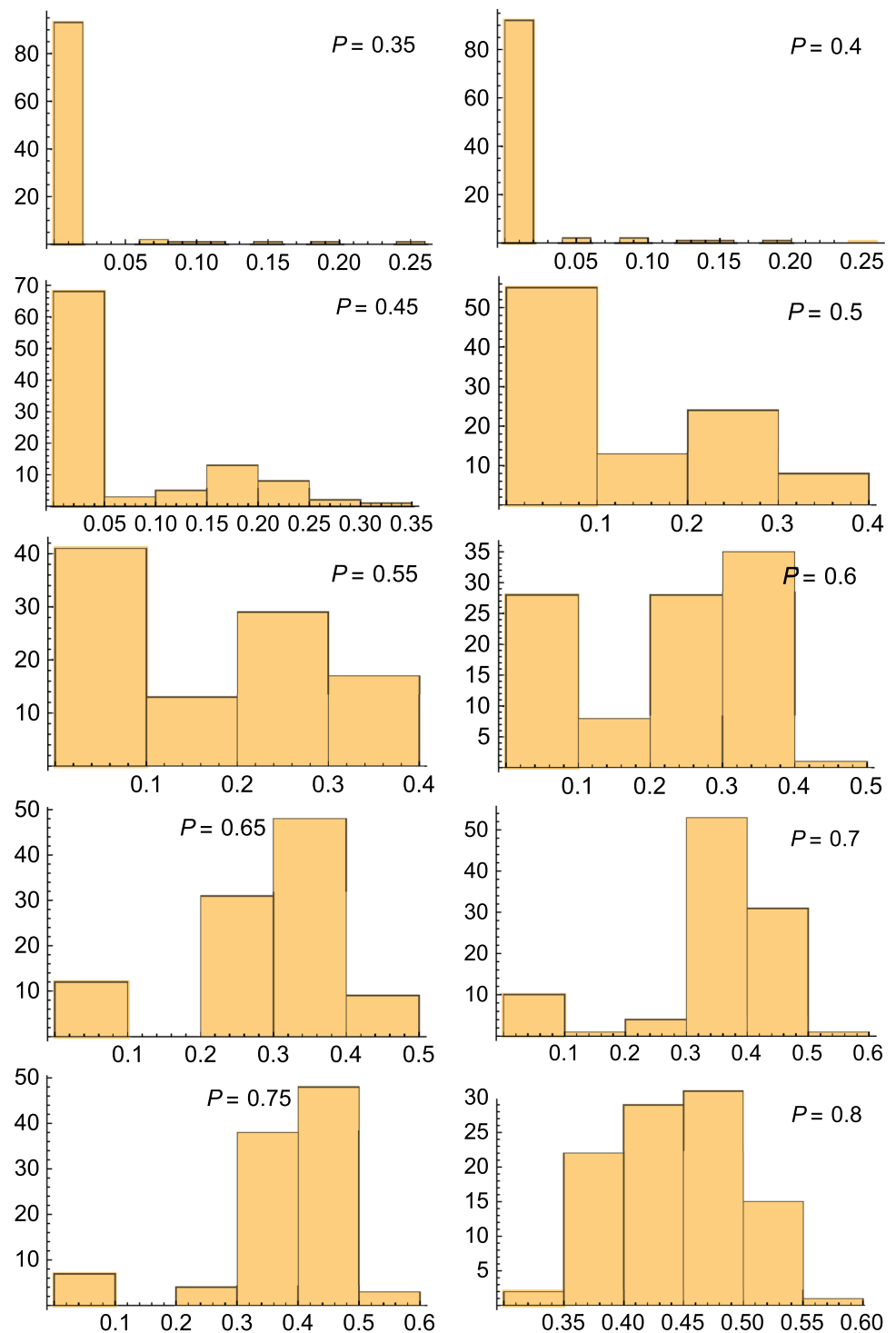
The computations were performed for  $q_{\min} = 0.2$ . The statistical estimations of the permeability for fixed  $P$  are presented in histograms selected in Figs. 10 and 11. The main features of these histograms are similar to the case of equal windows, including two peak plots.

The comparison of the fixed and random sizes window is given in Fig. 12. The following linear function fits the points on the interval (0.3, 1) from Table 2:

$$K = -0.339873 + 0.948525P. \tag{15}$$

It is worth noting that Eqs. (13) multiplied by 0.6 and (15) give almost the same results. This observation allows us to conjecture that the permeability does not depend on the distribution sizes of windows and can be estimated by its mean value only. Here, 0.6 is the mean value of the random variable uniformly distributed in the interval (0.2, 1).

**Fig. 10** Distribution of permeability of 100 samples for a fixed  $P$  in the case of random respective sizes window uniformly distributed in the interval  $(0.2, 1)$



## 5 Discussion and conclusion

A novel network computational model for a 3D ceramic structure is developed. The characteristic geometric features of the ceramic structure favorable for liquid metal flow during the infiltration process are determined. We combine two previously developed approaches, random network model

[29, 30], and structural approximation [36, 37]. More precisely, we apply the structural approximation and constructive homogenization method to the discrete stationary Stokes equations on random networks. Such an approach gives a robust algorithm to determine the macroscopic permeability  $K$  of IPCs. Besides the standard study of connectivity of random networks, the dependencies of  $K$  on random

Fig. 11 Continuation of Fig. 10

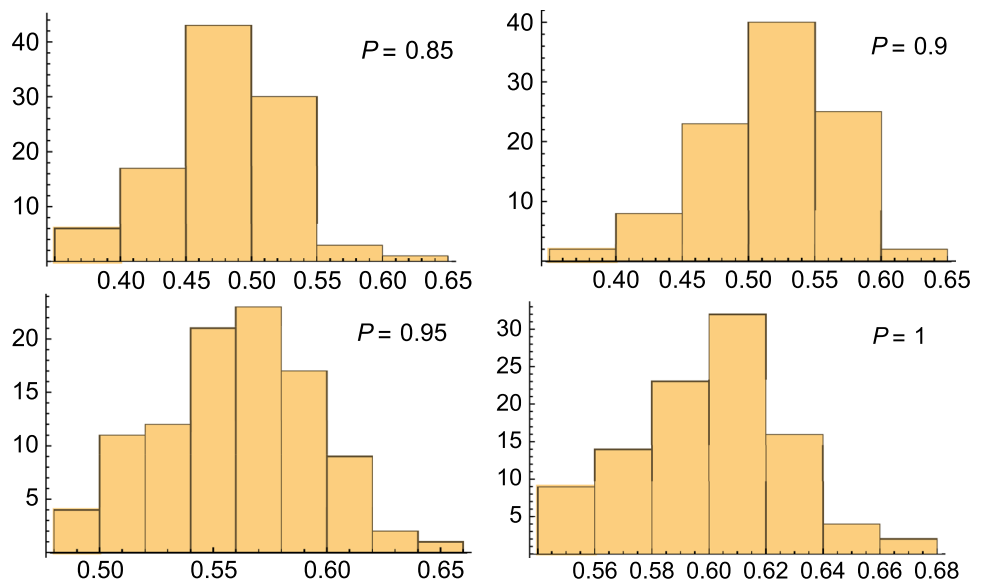


**Table 2** The statistical data of permeability  $K$  averaged over 100 numerical experiments with the random size of the window, the empirical mean value  $\mathbb{E}[K]$ , and the standard deviation  $\mathbb{D}[K]$  of  $K$  for a fixed  $P$

$P$	$\mathbb{E}[K]$	$\mathbb{D}[K]$
0.30	0.004340	0.024931
0.35	0.009022	0.037091
0.40	0.009961	0.038996
0.45	0.058510	0.090892
0.50	0.103848	0.121527
0.55	0.137360	0.139141
0.60	0.210660	0.142230
0.65	0.286792	0.119846
0.70	0.341205	0.125487
0.75	0.372791	0.117989
0.80	0.443062	0.051808
0.85	0.479934	0.047476
0.90	0.515980	0.050035
0.95	0.559472	0.034625
1.00	0.600705	0.026013

connections between the cells are derived; see Figs. 8 and 10. These histograms, including two observed peaks, can be useful in technological study, since the preliminary selection of porous preforms intended to produce IPC composites can be optimized for the low-pressure infiltration processes. The numerical simulations demonstrate that the permeability  $K$  does not depend on the scaled distribution sizes of windows; see Figs. 9 and 12. This yields a simple estimation of  $K$  by its mean value.

The present work complements and extends the previous research outlined in the Introduction, which concentrated on the local transport properties of tubes connecting the cells. For instance, the formula (35) from [32] shows that the permeability  $K$  is proportional to  $h = \frac{\langle d^2 \rangle}{\langle d^3 \rangle}$  where  $d$  denotes the diameter of window. The average over all the windows is used in the above equation. The formula (35) from [32] does not contain a network parameter; its randomness is expressed only by the coefficient  $h$ . This is a typical result of the simplified homogenization methodology when the main attention is paid to the local field, not to high-order averaging. In the present approach, we estimate the local field, so that the coefficient  $h$  is proportional to the window area, i.e.,  $h_1 = \langle d^2 \rangle$ . At the same time, we derive the dependence of  $K$  on the statistical parameters of networks. A similar investigation in the theory of dispersed composites by asymptotic [46] and Schwarz's [34] methods establishes a weak dependence on the macroscopic properties of local fields and a strong dependence on the geometric structure of composite. Maybe,  $h_1$  should be replaced by  $h$ . This implies the change of the uniform distribution used in Sect. 4.3. Maybe, the coefficient  $h$  should be calculated by more complicated expressions derived in [15] and others. Anyway, the previous local

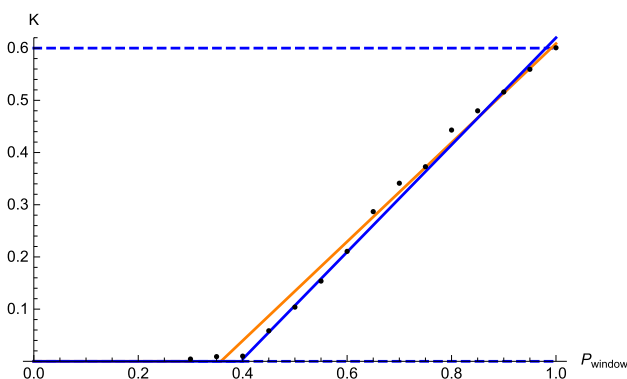


**Fig. 12** The dependence of the averaged permeability from Table 2 on the window probability  $P$ . The linear function (15) fitting the points on the interval (0.3, 1) is shown in orange. The function (13) multiplied by 0.6 is shown in blue

estimations can be combined with the developed network model to determine the permeability  $K$  for complex networks and complex shapes of local connections (tubes).

In the present paper, performing Monte Carlo simulations involved running thousands of computational experiments. The simulations were executed on a standard laptop to generate the results within minutes. This advantage of structural approximation over other locally effective numerical methods lies in its ability to enable a more efficient discretization approach. By concentrating on the key points of the physical process rather than relying on total discretization, structural approximation yields fast estimation of the macroscopic properties of complex random structures. Moreover, the proper application of constructive homogenization [34] prevents systematic errors arising during locally used effective medium approximations.

The discussion concerns the normalized permeability  $K$  calculated for dimensionless geometric structures. To apply the results to the dimensional ceramic foams, one has to multiply  $K$  by the corresponding value of dimension  $m^2$ . Based on experimental studies, it has been shown that the total porosity of the composites decreases with an increase in the window diameter  $d$  in the ceramic cell, and thus, the degree of infiltration process increases [12]. The experimental part of the study, complemented by simulations carried out in the present paper, will be continued and reported in a separate article devoted to technological applications.

**Acknowledgements** The research was supported by the Department of Materials Technology at the Silesian University of Technology, within the frame of the statutory research under Grant No. 11/030/BK\_23/1127 (BK-220/RM3/2023).

## Declarations

**Conflict of interest** All authors declared that they have no conflict of interest. The authors have no financial or proprietary interests in any material discussed in this article.

**Ethical approval** This article does not contain any studies with human participants or animals performed by any of the authors.

**Informed consent** Informed consent was obtained from all individual participants included in the study.

**Open Access** This article is licensed under a Creative Commons Attribution 4.0 International License, which permits use, sharing, adaptation, distribution and reproduction in any medium or format, as long as you give appropriate credit to the original author(s) and the source, provide a link to the Creative Commons licence, and indicate if changes were made. The images or other third party material in this article are included in the article's Creative Commons licence, unless indicated otherwise in a credit line to the material. If material is not included in the article's Creative Commons licence and your intended use is not permitted by statutory regulation or exceeds the permitted use, you will need to obtain permission directly from the copyright holder. To view a copy of this licence, visit <http://creativecommons.org/licenses/by/4.0/>.

## References

- Dolata AJ. Hybrid composites shaped by casting methods. *Solid State Phenom.* 2014;211:47–52.
- Olszówka-Myalska A, Myalski J. Applying stir casting method for mg alloy-short carbon fiber composite processing. *Compos Theory Pract.* 2019;14:81–5.
- Kota N, Charan MS, Laha T, Roy S. Review on development of metal/ceramic interpenetrating phase composites and critical analysis of their properties. *Ceram Int.* 2022;48(2):1451–83.
- Dolata AJ. Fabrication and structure characterization of alumina-aluminum interpenetrating phase composites. *J Mater Eng Perform.* 2016;25:3098–106. <https://doi.org/10.1007/s11665-016-1901-2>.
- Boczkowska A, Chabera P, Dolata AJ, Dyzia M, Kozera R, Oziębło A. Fabrication of ceramic-metal composites with percolation of phases using gpi. *Solid State Phenom.* 2012;191:57–66.
- Liu PS, Chen GF. General introduction to porous materials. In: Liu PS, Chen GF, editors. *Porous materials*. Boston: Butterworth-Heinemann; 2014. p. 1–20. <https://doi.org/10.1016/B978-0-12-407788-1.00001-0>.
- Kozera P, Boczkowska A, Kozera R, Małek M, Idczak W. The influence of the microstructure of ceramic-elastomer composites on their energy absorption capability. *Materials.* 2021. <https://doi.org/10.3390/ma14216618>.
- Binner J, Chang H, Higginson R. Processing of ceramic-metal interpenetrating composites. *J Eur Ceram Soc.* 2009;29:837–42. <https://doi.org/10.1016/j.jeurceramsoc.2008.07.034>.
- Colombo P. Conventional and novel processing methods for cellular ceramics. *Philos Trans Ser A Math Phys Eng Sci.* 2006;364:109–24. <https://doi.org/10.1098/rsta.2005.1683>.
- Stuart AR, Gonzenbach UT, Tervoort E, Gauckler LJ. Processing routes to macroporous ceramics: a review. *J Am Ceram Soc.* 2006;89(6):1771–89. <https://doi.org/10.1111/j.1551-2916.2006.01044.x> (<https://ceramics.onlinelibrary.wiley.com/doi/pdf/10.1111/j.1551-2916.2006.01044.x>).
- Tulliani J-M, Lombardi M, Palmero P, Fornabaio M, Gibson LJ. Development and mechanical characterization of novel ceramic foams fabricated by gel-casting. *J Eur Ceram Soc.* 2013;33:1567–76. <https://doi.org/10.1016/j.jeurceramsoc.2013.01.038>.
- Dolata AJ, Dyzia M, Jaegermann A. Structure and physical properties of alumina ceramic foams designed for centrifugal infiltration process. *Compos Theory Pract.* 2017;17(3):136–43.
- Dolata AJ. Centrifugal infiltration of porous ceramic preforms by the liquid alloy—theoretical background and experimental verification. *Arch Metall Mater.* 2016. <https://doi.org/10.1515/amm-2016-0075>.
- Conway JH, Sloane NJA. *Sphere packings, lattices and groups*, vol. 290. New York: Springer; 2013.
- Malevich A, Mityushev V, Adler P. Stokes flow through a channel with wavy walls. *Acta Mech.* 2006;182:151–82. <https://doi.org/10.1007/s00707-005-0293-4>.
- Scholle M, Mellmann M, Gaskell PH, Westerkamp L, Marnier F. Multilayer modelling of lubricated contacts: a new approach based on a potential field description. Berlin: Springer; 2020.
- Birkert A, Hartmann B, Scholle M, Straub M. Optimization of the process robustness of the stamping of complex body parts with regard to dimensional accuracy. *IOP Conf Ser Mater Sci Eng.* 2018;418: 012107. <https://doi.org/10.1088/1757-899x/418/1/012107>.
- Bakhvalov NS, Panasenko G. Homogenisation: averaging processes in periodic media: mathematical problems in the mechanics of composite materials, vol. 36. Berlin: Springer; 2012.

19. Auriault J-L. Transient heat and solute transfers in liquid-saturated porous media. *Transp Porous Media*. 2016;115(1):63–78. <https://doi.org/10.1007/s11242-016-0753-4>.
20. Mikelić A. Homogenization theory and applications to filtration through porous media. In: Fasano, A. editor. *Filtration in Porous Media and Industrial Application: Lectures Given at the 4th Session of the Centro Internazionale Matematico Estivo (C.I.M.E.) Held in Cetraro, Italy August 24–29*. Berlin: Springer; 1998. p. 127–214 (2000). <https://doi.org/10.1007/BFb0103977>.
21. Craster RV, Kaplunov J, Postnova J. High-frequency asymptotics, homogenisation and localisation for lattices. *Q J Mech Appl Math*. 2010;63(4):497–519. <https://doi.org/10.1093/qjmam/hbq015> (<https://academic.oup.com/qjmam/article-pdf/63/4/497/5371907/hbq015.pdf>).
22. Craster RV, Joseph LM, Kaplunov J. Long-wave asymptotic theories: the connection between functionally graded waveguides and periodic media. *Wave Motion*. 2014;51(4):581–8. <https://doi.org/10.1016/j.wavemoti.2013.09.007>. (**Innovations in Wave Modelling**).
23. Farina A, Fusi L, Mikelić A, Saccomandi G, Sequeira A, Toro EF, Mikelić A. An introduction to the homogenization modeling of non-newtonian and electrokinetic flows in porous media. *Non-Newtonian Fluid Mechanics and Complex Flows: Levico Terme, Italy*. 2018;2016. p. 171–227.
24. Adler P, Thovert J-F, Mourzenko V. *Fractured porous media*. Oxford: Oxford University Press; 2013. <https://doi.org/10.1093/acprof:oso/9780199666515.001.0001>.
25. Mourzenko V, Thovert J-F, Adler P. Conductivity and transmissivity of a single fracture. *Transp Porous Media*. 2018;123(2):235–56. <https://doi.org/10.1007/s11242-018-1037-y>.
26. Thovert J-F, Mourzenko VV, Adler PM. Percolation in three-dimensional fracture networks for arbitrary size and shape distributions. *Phys Rev E*. 2017;95: 042112. <https://doi.org/10.1103/PhysRevE.95.042112>.
27. Hunt A, Ewing R, Ghanbarian B. *Percolation theory for flow in porous media*, vol. 880. Berlin: Springer; 2014.
28. Payatakes AC, Tien C, Turian RM. A new model for granular porous media: part i. Model formulation. *AIChE J*. 1973;19(1):58–67.
29. Constantinides GN, Payatakes AC. A three dimensional network model for consolidated porous media. *Basic studies*. *Chem Eng Commun*. 1989;81(1):55–81.
30. Valavanides MS. Oil fragmentation, interfacial surface transport and flow structure maps for two-phase flow in model pore networks. predictions based on extensive, deprof model simulations. *Oil & Gas Sciences and Technology—Revue d'IFP Energies nouvelles*, vol. 73. 2018. p. 6.
31. Acosta GF, Castillejos EA, Almanza RJ, Flores VA, et al. Analysis of liquid flow through ceramic porous media used for molten metal filtration. *Metall Mater Trans B*. 1995;26(1):159–71.
32. Agrawal P, Mascini A, Bultreys T, Aslannejad H, Wolthers M, Cnudde V, Butler IB, Raouf A. The impact of pore-throat shape evolution during dissolution on carbonate rock permeability: pore network modeling and experiments. *Adv Water Resour*. 2021;155: 103991.
33. Valavanides MS, Payatakes AC. Effects of pore network characteristics on steady-state two-phase flow based on a true-to-mechanism model (deprof). In: Abu Dhabi International Petroleum Exhibition and Conference (2002). OnePetro
34. Mityushev V. Effective properties of two-dimensional dispersed composites. Part ii. Revision of self-consistent methods. *Comput Math Appl*. 2022;121:74–84.
35. Drygaś P, Gluzman S, Mityushev V, Nawalaniec W. *Applied analysis of composite media: analytical and computational results for materials scientists and engineers*. Duxford: Woodhead Publishing; 2019.
36. Berlyand L, Kolpakov AG, Novikov A. *Introduction to the network approximation method for materials modeling*. *Encyclopedia of mathematics and its applications*. Cambridge: Cambridge University Press; 2013.
37. Kolpakov AA, Kolpakov AG. *Capacity and transport in contrast composite structures: asymptotic analysis and applications*. Boca Raton: CRC Press; 2009. <https://doi.org/10.1201/9781439801765>.
38. Nawalaniec W, Necka K, Mityushev V. Effective conductivity of densely packed disks and energy of graphs. *Mathematics*. 2020;8(12):2161.
39. Moller J. *Lectures on random Voronoi tessellations*, vol. 87. Berlin: Springer; 2012.
40. Jikov VV, Kozlov SM, Oleinik OA. *Homogenization of differential operators and integral functionals*. Berlin: Springer; 2012.
41. Castañeda PP, Telega JJ, Gambin B. *Nonlinear homogenization and its applications to composites, polycrystals and smart materials: proceedings of the NATO advanced research workshop, held in Warsaw, Poland, 23–26 June 2003*, vol 170. Springer, Berlin (2004)
42. Gluzman S, Mityushev V, Nawalaniec W. *Computational analysis of structured media*. Oxford: Academic Press; 2017.
43. Gallier J. *Geometric methods and applications: for computer science and engineering*, vol. 38. Berlin: Springer; 2011.
44. Temam R. *Navier–Stokes equations: theory and numerical analysis*, vol. 343. Rhode Island: American Mathematical Soc; 2001.
45. Grigor'yan A. *Introduction to analysis on graphs*, vol. 71. Rhode Island: AMS; 2018.
46. Mityushev V, Rylko N. Maxwell's approach to effective conductivity and its limitations. *Q J Mech Appl Math*. 2013;66(2):241–51.

**Publisher's Note** Springer Nature remains neutral with regard to jurisdictional claims in published maps and institutional affiliations.